

# A Nonlinear System Science Approach to Find the Robust Solar Wind Drivers of the Multivariate Magnetosphere

Sylvain Blunier<sup>1</sup>, Benjamin Toledo<sup>1</sup>, Jose Rogan<sup>1</sup>, and Juan Alejandro Valdivia<sup>1</sup>

<sup>1</sup>Universidad de Chile

November 22, 2022

## Abstract

We propose a method, based on Neural Networks, that detects the nonlinear robust interplanetary solar wind variables, with varying delays, driving the coupled behavior of three geomagnetic indices (Dst, AL, and AU). As opposed to minimizing a prediction error, the method is based on degrading the prediction by distorting the inputs of the trained Neural Networks in order to highlight the most sensible drivers. We show that the  $B_z$  component of the magnetic field, the duskward oriented electric field, and the speed of the particles of the interplanetary medium, at particular time delays, seem to be the most efficient drivers of the three coupled geomagnetic indices. Using only the sensible or robust drivers in the model, we demonstrate that iterated predictions during geomagnetic storm are significantly improved from models that only use one of the outstanding drivers with multiple time delays. The derived robust nonlinear Neural Network model is also a significant improvement over linear approximations, specially when used as iterated predictors.

1 **A Nonlinear System Science Approach to Find the**  
2 **Robust Solar Wind Drivers of the Multivariate**  
3 **Magnetosphere**

4 **S. Blunier<sup>1</sup>, B. Toledo<sup>1,2</sup>, J. Rogan<sup>1,2</sup>, J. A. Valdivia<sup>1,2</sup>**

5 <sup>1</sup>Departamento de Física, Facultad de Ciencias, Universidad de Chile, Santiago, Chile

6 <sup>2</sup>Centro para el Desarrollo de la Nanociencia y Nanotecnología, CEDENNA, Santiago, Chile

## 7 Abstract

8 We propose a method, based on Neural Networks, that detects the nonlinear robust interplanetary solar wind variables, with varying delays, driving the coupled behavior of  
 9 three geomagnetic indices (Dst, AL, and AU). As opposed to minimizing a prediction  
 10 error, the method is based on degrading the prediction by distorting the inputs of the  
 11 trained Neural Networks in order to highlight the most sensible drivers. We show that  
 12 the  $z$  component of the magnetic field, the duskward oriented electric field, and the speed  
 13 of the particles of the interplanetary medium, at particular time delays, seem to be the  
 14 most efficient drivers of the three coupled geomagnetic indices. Using only the sensible  
 15 or robust drivers in the model, we demonstrate that iterated predictions during geomag-  
 16 netic storm are significantly improved from models that only use one of the outstand-  
 17 ing drivers with multiple time delays. The derived robust nonlinear Neural Network model  
 18 is also a significant improvement over linear approximations, specially when used as it-  
 19 iterated predictors.  
 20

## 21 1 Introduction

22 The study of the solar wind-magnetosphere-ionosphere (SWMI) coupled system has  
 23 become a relevant subject of wide interest, not only because of its scientific repercussions,  
 24 but also for its application in space weather forecasts (e.g. Hapgood (2018); Campore-  
 25 ale (2019); Bala and Reiff (2018)). As such, constructing models that are able to describe  
 26 certain characterizations of the SWMI system in a robust manner can have important  
 27 social and economical consequences for our countries, and the world in general, since space  
 28 weather can affect a number of human activities such as mining, natural disaster man-  
 29 agement, remote communications, precise farming, aircraft traffic communication, power  
 30 grid management, etc (e.g. Hapgood (2018); Council (2008)).

31 It is well known that the Sun activity can affect the Earth magnetosphere and iono-  
 32 sphere (Gosling, 2000). This can be quickly realized by observing the simultaneous evo-  
 33 lution of a number of solar wind parameters and magnetospheric indices that are used  
 34 to monitor the magnetospheric and ionospheric activity. For example the Disturbance  
 35 Storm-Time ( $Dst$ ) index is used to describe the horizontal magnetic field variations close  
 36 to the magnetic equator. Hourly  $Dst$  indices since 1957 have been derived by Sugiura  
 37 (1964), and more recently, they are available, in real-time, at the World Data Center in  
 38 Kyoto in Japan. The  $Dst$  is likely the most studied index in relation to geomagnetic storms,  
 39 for example, Burton et al. (1975) constructed a linear evolution model driven by the so-  
 40 lar wind  $VB_s$  and dynamic pressure  $P$ . Here  $V$  is the bulk ion velocity,  $B_s$  is the south-  
 41 ward component of the interplanetary magnetic field. Further studies and discussions  
 42 suggested that the  $Dst$  evolution may be nonlinear (J. A. Valdivia et al., 1996; Vassil-  
 43 iadis et al., 1999) and that more magnetospheric and solarwind variables should be con-  
 44 sidered to represent storm time space-weather phenomena (Borovsky & Shprits, 2017;  
 45 Borovsky, 2020).

46 Similarly, the upper AU and lower AL auroral indices, representing the envelopes  
 47 of the magnetic fields variations taken from around 12 high latitude geomagnetic obser-  
 48 vatories (Davis & Sugiura, 1966), provide complementary information about a different  
 49 region of the SWMI system. There has been a number of studies that strongly suggest  
 50 that the solar wind driven dynamics of AL and AU are nonlinear (Bargatze et al., 1985;  
 51 Vassiliadis et al., 1995, 2000).

52 Furthermore, a system science approach very quickly reveals that there are com-  
 53 plex interactions among the different regions of the magnetosphere and the solar wind (Borovsky  
 54 & Valdivia, 2018). Hence, the inherent complexity of the SWMI system (J. A. Valdivia  
 55 et al., 2005; J. Valdivia et al., 2013; Consolini et al., 2018; Donner et al., 2019), demands  
 56 the development of models and techniques to account for these interactions in a robust  
 57 manner.

58 This is becoming particularly true as we are increasingly relying on artificial in-  
 59 telligence models to try to account for such complex behavior (Bortnik et al., 2018; Jawad  
 60 et al., 2019). However, when developing robust models, it is not enough to just train a  
 61 neural net with a large number of variables since, given the complex and nonlinear nature  
 62 of the system, the model will probably not work as efficient on a set of events that  
 63 is different from the training set. Therefore, we need to identify what are the robust vari-  
 64 ables, among all accessible ones, that should be included when constructing a simplified  
 65 representation of the SWMI system such that it still works on a different set of events.

66 Hence, a robust multivariate nonlinear system science description, that for exam-  
 67 ple includes the coupling of these 3 magnetospheric indices (MI) and with solar wind drivers (Borovsky  
 68 & Denton, 2018; J. A. Valdivia et al., 1999) can further our understanding of these in-  
 69 teractions and their time scales (Adhikari et al., 2020), and could pave the way to ro-  
 70 bust Space Weather applications. This is what we are going to start analyzing in this  
 71 manuscript. So that, for simplicity, we will study the 3 above described geomagnetic or  
 72 magnetospheric indices (MI) ( $Dst(t)$ ,  $AL(t)$  and  $AU(t)$ ) and search for the robust solar  
 73 wind variables (SWV), and their possible time delays, that drive the magnetosphere re-  
 74 sponse as characterized by these 3 indices. In our study we will consider data with an  
 75 hour time scale and let faster variation to future work.

76 As a model reconstruction, we will use Neural Networks (NN) because they have  
 77 demonstrated to be a powerful machine learning tool capable of performing complex tasks  
 78 (Abiodun et al., 2018). NN have already been used to forecast the  $Dst$  index (Lazzus  
 79 et al., 2017; Gruet et al., 2018) showing that it has a high self correlation with the im-  
 80 mediate past measurements, therefore, the NN will include the  $Dst$  index at time  $t$  as  
 81 part of the NN variables. The same will be done for the other magnetospheric indices  
 82 that we are considering here.

83 A huge advantage of NN is their capability to build functions that can be highly  
 84 non-linear and that property is the one we want to exploit in the present study. The coun-  
 85 terpart is that once they are trained, they are a black box which parameters remain mean-  
 86 ingless to humans. We are therefore strongly limited to extract valuable physical infor-  
 87 mation from what they could have “learned”. Furthermore, it is very common that their  
 88 predictability could be quite high in the training set, but not as good in out-of-sample  
 89 forecasting of other events. In the present manuscript we purpose a method that quan-  
 90 tifies the robustness of a solar wind variable as the degradation of the predictability of  
 91 the trained model when such a variable is perturbed trying to forecast a different test-  
 92 ing set of events. The most sensitive or robust variables, are those which produce the  
 93 largest error when perturbed over the testing set.

94 In the present study we address the model construction in two ways. First we con-  
 95 sider a short term prediction that uses the selected solar wind variables, and their de-  
 96 lays, at a particular moment in order to predict the geomagnetic indices for the next hour,  
 97 which we call *one step forecasting*. The second way is to use the one step prediction model  
 98 to forecast the MI for a longer time interval, using the selected SWV, and their time de-  
 99 lays, and reinserting the predicted geomagnetic indices in the model, which we will call  
 100 *iterated forecasting*.

101 In order to simulate real-time forecasting we use the *iterated forecasting*, since we  
 102 note that some of these indices are not easily accessible in real time or are available only  
 103 part of the time.

104 If successful, our approach would provide a strong indication that the selected ro-  
 105 bust inputs drive the signal and brings information about the physics of the system. This  
 106 information could be used as a complementary approach to test, validate, and optimize  
 107 forecasting models of the magnetospheric response to solar wind input, and in general  
 108 of any driven complex system under study. For example, predictions of the  $Dst$  index

109 are provided by many services like the Space Weather Center Prediction, or `www.spaceweatherlive`  
 110 `.com`. Their short term accuracy could be tested, improved, and optimize by following  
 111 our strategy to find robust modes of interaction. Additionally, since our strategy of con-  
 112 structing these forecasting models is quite different from the standard ones, it is always  
 113 useful to provide an alternative forecast, specially during periods where real-time *Dst*  
 114 may not be available. The same can be said about AL and AU, which are usually not  
 115 easily available in real time.

## 116 2 Data description

117 The values of the *Dst* index are provided hourly from year 1957 to the present at  
 118 the World Data Center for Geomagnetism in Kyoto, they can be found at `http://wdc`  
 119 `.kugi.kyoto-u.ac.jp/dst/dir/index.html` ((Masahito et al., 2015)). No value is miss-  
 120 ing since 1957, thus no signal reconstruction is needed. We will then use the hourly res-  
 121 olution in all the study Data of interplanetary medium and the AU and AL indices where  
 122 retrieved from the OMNI database provided by the National Aeeronautic and Spatial  
 123 Agency and freely available at `ftp://spdf.gsfc.nasa.gov/pub/data/omni/high_res`  
 124 `_omni/` ((King & Papitashvili, 2005)). The oldest available data in OMNI is from 1963  
 125 but with an average data rate lower than 20% which is too sporadic for our purposes.  
 126 From year 1995 the data rate improved significantly thanks to the Wind and ACE satel-  
 127 lites commissioning.

128 OMNI data are provided with a resolution of one minute but are not continuous.  
 129 Since *Dst* is provided hourly, we choose to perform this study using a resolution of one  
 130 hour, therefore OMNI data need to be transformed to one hour sampling. Values are taken  
 131 when the UTC minute is equal to 0 and will be calculated as the average over all avail-  
 132 able data of the 60 following minutes. Even if only one value is available during this hour  
 133 it will be taken as the value of the corresponding hour. In case no data is provided dur-  
 134 ing this interval, they will be generated with by a linear interpolation from the available  
 135 values.

136 The SWV that we use from the OMNI database are the three interplanetary mag-  
 137 netic field (IMF) components given in the GSE coordinate system ( $B_x, B_y, B_z$ ), the par-  
 138 ticle flow speed ( $V$ ), the proton number density ( $N$ ), the plasma temperature ( $T$ ), and  
 139 the proton dynamical pressure ( $p$ ). It is worth noticing that  $p$  is not a direct measure-  
 140 ment but it is calculated from the proton speed and density by  $p = 2 \times 10^{-6} NV^2$  (nPa).  
 141 We can also construct composed variables that will be considered in the analysis. One  
 142 is  $VB_s$ , where  $B_s$  is the negative component of  $B_z$ , so that it is zero if  $B_z > 0$  and  $B_z$   
 143 if  $B_z < 0$ . Sometimes, people prefer to write this expression in the GSM coordinate sys-  
 144 tem, but for our purpose we stay within the GSE coordinate system just to demonstrate  
 145 that we can include composed indexes in the analysis. Similarly, we define  $\varepsilon_A = VB^2 \sin^4(\theta/2) l_0^2$ ,  
 146 where  $B$  as the magnitude of the IMF,  $l_0$  is seven times the Earth radii, and the clock  
 147 angle  $\theta$  is  $\tan^{-1}(|B_y/B_z|)$  for  $B_z > 0$  and  $\pi - \tan^{-1}(|B_y/B_z|)$  for  $B_z < 0$ . When us-  
 148 ing variables in the GSM coordinate system, such formula would describe the Akasofu's  
 149 index.

150 All the used interplanetary variable are summarized in Table 1 with their units and  
 151 typical values in quiet and disturbed times, they will all be treated as independent vari-  
 152 ables.

153 Since we are interested in studying perturbations of the magnetosphere, we will con-  
 154 centrate on geomagnetic storms intervals where the *Dst* index reach a climax below  $-100$  nT.  
 155 We consider the storm is over the first time that *Dst* reach  $Dst_{end} > -10$  nT after the  
 156 climax. The beginning of the storm is taken  $T_b$  hours before the climax, such that  $T_b$  is  
 157 20% of the time that separates the climax to the end of the storm. Between 1995 and  
 158 2018 we identify 97 geomagnetic storms that reach a climax below  $-100$  nT. In order

SW signal	Symbol	Quiet	Storm	Unit
3 Magnetic field components	$B_{x,y,z}$	$ B_{x,y,z}  \leq 10$	$ B_{x,y,z}  > 10$	nT
Flow speed	$V$	300 – 400	> 500	$\text{km s}^{-1}$
$VB_s$ parameter	$VB_s$	0	< -4000	$\mu\text{V s}^{-1}$
Pressure	$P$	0 – 5	> 5	nPa
Temperature	$T$	$10^4 - 10^5$	$> 2 \times 10^5$	K
Number density	$N$	1 – 10	> 15	# particles/cc
$\epsilon_A$ parameter	$\epsilon_A$	$< 10^{11}$	$> 10^{11}$	Watt

**Table 1.** Solar wind variables that are analyzed for their capability to drive the geomagnetic indices considered here. We give their mathematical symbol, their typical values during quiet and active periods, and their units. To be used for the neural net analysis, all variables will be mapped to the range between  $[0, 1]$ , so their absolute values and units will not be extremely relevant in the rest of the development.

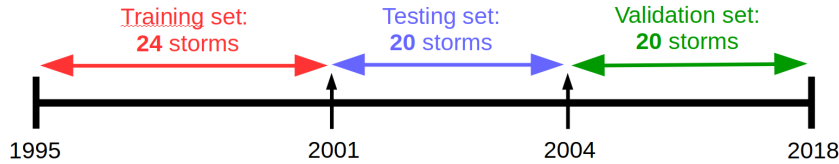


**Figure 1.** Separation of storms for training, testing, and validation sets, the first 24 storms will be used for training, the following 20 storms for the testing phase, and the last 20 storms for the validation step.

159 to improve the robustness of the data we require that all the variables used during the  
 160 time of the storm fulfill with the following criteria: (a) a maximum of 5 continuous hours  
 161 with no data, and (b) at least 90% of data available during the storm interval. After ap-  
 162 plying those filters we have a set of 64 storms between 1995 and 2018 that will be used  
 163 for our study.

### 164 3 Analysis

165 The 64 selected storms are split in training, testing, and validation sets as described  
 166 in figure 1. In order to train and test our NN we use the Keras library under python.  
 167 All data are scaled with the *MinMaxScaler* from the python *sklearn* library.

168 For the training phase we use the default Keras binary cross entropy loss function  
 169 defined as:

$$C = -\frac{1}{N} \sum_{j=1}^{N_{out}} [y_j \ln \hat{y}_j^L + (1 - y_j) \ln(1 - \hat{y}_j^L)],$$

170 where  $N_{out}$  corresponds to the number of outputs of the NN,  $y_j$  are the normal-  
 171 ized data values,  $\hat{y}_j$  are the normalized output predicted by the NN. This function is non-  
 172 negative and converge to zero when  $\hat{y}_j$  gets closer to  $y_j$ . The minimization if performed  
 173 with the Keras *adam* optimizer.

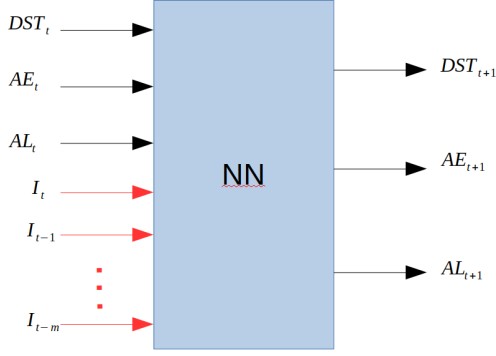


**Figure 2.** Input/Output variables used to train and test the NN in the case of a single solar wind driver ( $n = 1$ ). The general case with multiple solar wind drivers follows the same pattern. Note that the magnetospheric variables in the evolution model are considered, for simplicity, only at the previous time  $t$ . This will be generalized in a future work.

174 All our NN have 3 hidden layers of 100 neurons activated with a sigmoid function.  
 175 This allows us to describe a reasonably complex evolution function, given by

$$\bar{\mathbf{G}}_{t+1} = NN(\mathbf{G}_t, \mathbf{I}_t), \quad (1)$$

176 which gives us the value of the GI at  $t + 1$  from information at previous times. From  
 177 now on, the bar on top of a variable means it is generated by the NN model. Here  $\mathbf{G}_t$   
 178 corresponds to the magnetospheric vector

$$\mathbf{G}_t = (Dst_t, AU_t, AL_t),$$

179 while  $\mathbf{I}_t$  corresponds to a set of solar wind drivers, possibly at different time delays, namely

$$\mathbf{I}_t = (I_{1,t-1}, \dots, I_{1,t-m_1}, \dots, I_{n,t-1}, \dots, I_{n,t-m_n}),$$

180 where  $I_{n,t}$  is the  $n^{th}$  solar wind driver at time  $t$ . The 9 solar wind drivers are described  
 181 in table 1 and we will study their capability to robustly drive  $\mathbf{G}_t$ . In our study we will  
 182 take, at most,  $m_i = m = 10$  for all solar wind drivers, so that we will be able to check  
 183 the influence of each solar wind driver on the magnetospheric variables up to 10 hours  
 184 in the past. The NN is trained to make one step forecasting using the evolution func-  
 185 tion given by Eq. 1. The global structure of the NN for the training and testing phases  
 186 is represented in Fig. 2.

187 In order to avoid over-fitting, at each epoch of the training phase, the cross entropy  
 188 function is calculated using data from the testing set and is compared with the last best  
 189 result obtained during the minimization. At each step, if the NN is better than the last  
 190 best NN, it replaces it. This minimization process runs over 400 epochs, thus the NN  
 191 corresponding to the last best epoch will be saved.

192 One of the difficulties of training NNs with real data is the multiple solution that  
 193 can be found by the algorithm. The minimizing process can stabilize around a bad lo-  
 194 cal minimum and then will miss the optimal solution. The best model of geomagnetic  
 195 behavior prediction should be the NN that provides the lowest errors, even if we can-  
 196 not guarantee that the algorithm has actually found the best solution. For each SWV  
 197 of Table 1, we train around 40 NN and keep the best one for the testing phase.

198 In order to evaluate our models, we compare it to the toy model  $\bar{\mathbf{G}}_{t+1}^p = \mathbf{G}_t$  that  
 199 we call persistence model. For the testing and validation phases we compute the unit-  
 200 less mean absolute error (MAE) of a particular geomagnetic index  $X_t$ , normalized by the

201 error calculated in the persistence model, namely,

$$\epsilon_{MAE} = \frac{\sum_{t_i=1}^{t_f} |\bar{X}_{t+1} - X_{t+1}|}{\sum_{t_i=1}^{t_f} |\bar{X}_{t+1}^p - X_{t+1}|}. \quad (2)$$

202 The advantage of this measure is that it provides a direct comparison with the per-  
 203 sistence model, but it also gives equal relevance to all the magnetospheric indices when  
 204 we add the MAE for the 3 of them.

205 In order to evaluate the contribution of a particular solar wind driver, with a par-  
 206 ticular time delay, we will add to it a Gaussian noise centered in 0 and with an increas-  
 207 ing standard deviation  $\sigma$ , such that the particular solar wind driver is now given by  $I_{i,t-j} \rightarrow$   
 208  $I_{i,t-j} + \delta_t^{(i,j)}$ . All the other solar wind drivers are not perturbed. Here,  $\sigma$  will vary from  
 209 0% to 100% of the difference between the maximum and the minimum values obtained  
 210 in the particular solar driver signal during the tested storm interval. If the NN is well  
 211 trained, the noised introduced to the particular solar wind driver, at the particular time  
 212 delay, is expected to degrade the prediction; and the higher the value of  $\sigma$ , the higher  
 213 should be the  $\epsilon_{MAE}$ . This will be called the noised input method. This analysis is then  
 214 repeated on the same NN but perturbing another solar wind driver and/or time delay.  
 215 We expect that the most robust solar wind drivers, at a particular time delay, are the  
 216 ones that are most sensitive to the perturbation giving the largest error. Here we report  
 217 the normalized MAE as  $\epsilon(\sigma)/\epsilon(0) - 1$  for each of the geomagnetic indices.

218 To start, we train a NN that contains the geomagnetic indices and only one solar  
 219 wind driver  $I_{i,t}$  over the training set. We then perturb the same solar wind driver over  
 220 the testing set, and observe its sensitivity with  $\sigma$ . We repeat the procedure for the other  
 221 solar wind drivers, as shown in Fig. 3a-c for the storm of March 2001 that reached a pick  
 222 value of  $-149$  nT for the  $Dst$  index.

223 For each trained NN that corresponds to a particular solar wind driver, the test-  
 224 ing phase is repeated 50 times for each  $\sigma$  and we keep the average of the obtained er-  
 225 ror. Since the error is centered, all the curves begin at 0 for  $\sigma = 0$ . The solar wind driver  
 226 is associated with one error per geomagnetic index. With this procedure, we expect to  
 227 gain information on the correlation of the disturbed solar wind driver and its capabil-  
 228 ity to predict  $\mathbf{G}_t$ .

229 We note that  $B_z$  and  $VB_s$  are consistently the most sensitive variables for the pre-  
 230 diction of these 3 geomagnetic indices, which we will denote them the robust solar wind  
 231 variables. For example, when the perturbations is of the size of the signal for  $Dst$ , mean-  
 232 ing with  $\sigma = 1$  the error is multiplied by 9 in the case of  $B_z$  and above 6 for  $VB_s$ , while  
 233 the other drivers show a much lower perturbation when the noise increases. For the AL  
 234 index, the effect is lower but still present, and  $B_z$  and  $VB_s$  remain by far the most sen-  
 235 sitive solar wind drivers. Although in the case of AU the error does not reach more than  
 236 100% from the clean input for any of the solar wind drivers, still  $B_z$  and  $VB_s$  show up  
 237 as relevant. Of course, for AU other variables could also be relevant such as density. Hence,  
 238 we obtain an error for each geomagnetic index given a value of  $\sigma$  that informs us about  
 239 the global robustness of the solar wind driver in the NN, and therefore, about the global  
 240 robustness of this solar wind driver to predict  $\mathbf{G}_t$ . Let us note that the strategy we are  
 241 using to determine the robust solar wind variables may at first sight seem counter in-  
 242 tuitive, since we are not trying to minimize an error, but to maximize it. But after sub-  
 243 sequent consideration, we hope it becomes more clear.

244 In order to provide a more general conclusion we repeat the experiment 50 times  
 245 with  $\sigma(\%) = 1$  for each storm. We show the average error over all the storms for each  
 246 geomagnetic index and solar wind driver in Fig. 4. For a given magnetospheric index and  
 247 solar wind driver we have a bin that represents how perturbed is the error when the in-  
 248 put is noised, therefore, telling us about its contribution to the forecast. We also give

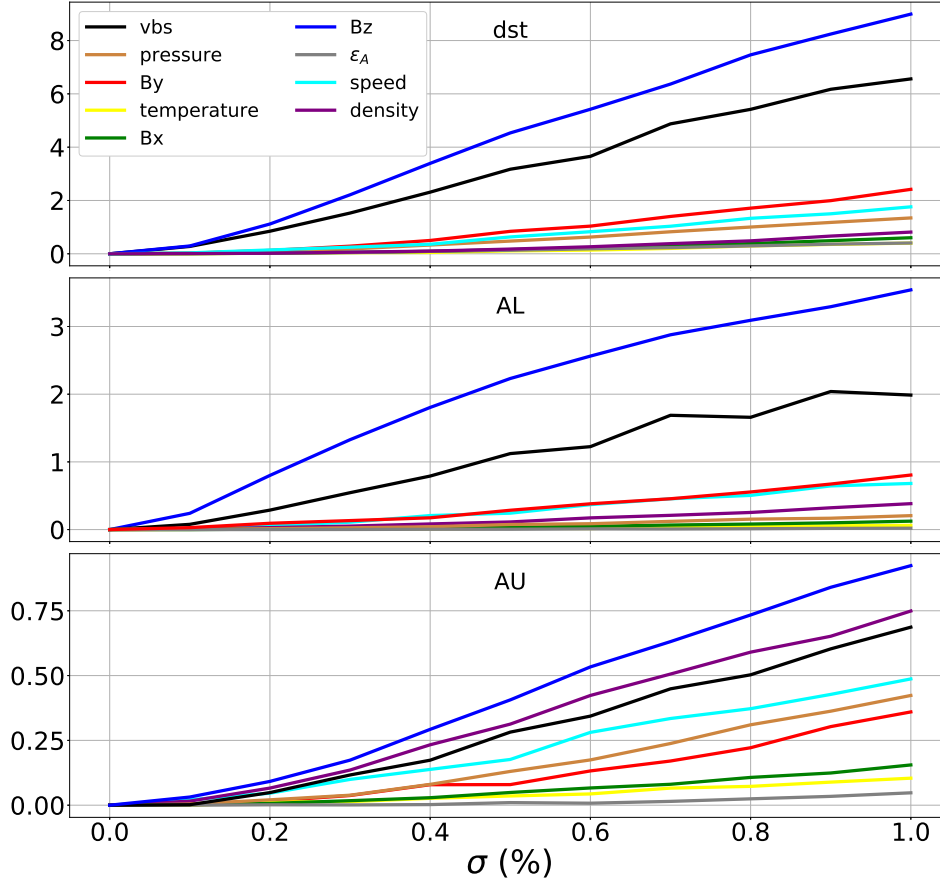


**Figure 3.** Evolution of the normalized MAE for each of the geomagnetic indices (a) Dst, (b) AL, and (c) AU with the amplitude of the noise  $\sigma$  during the storm of March 2001. The  $B_z$  and  $VB_s$  signals are consistently the most sensitive solar wind variables to the variation of  $\sigma$  while the others are not giving any strong evidence of contribution to the prediction.

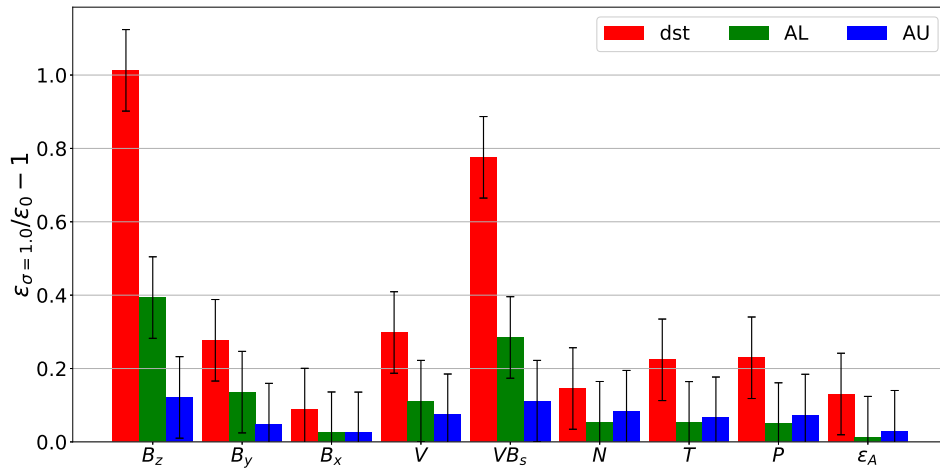


**Figure 4.** Summary of the response of each trained NN to the perturbed solar wind driver over all the storms in the testing set. The standard deviation of the error is also shown. We use 50 surrogates for each storm and solar wind driver. The most sensitive parameters are clearly  $B_z$  and  $VB_s$ .

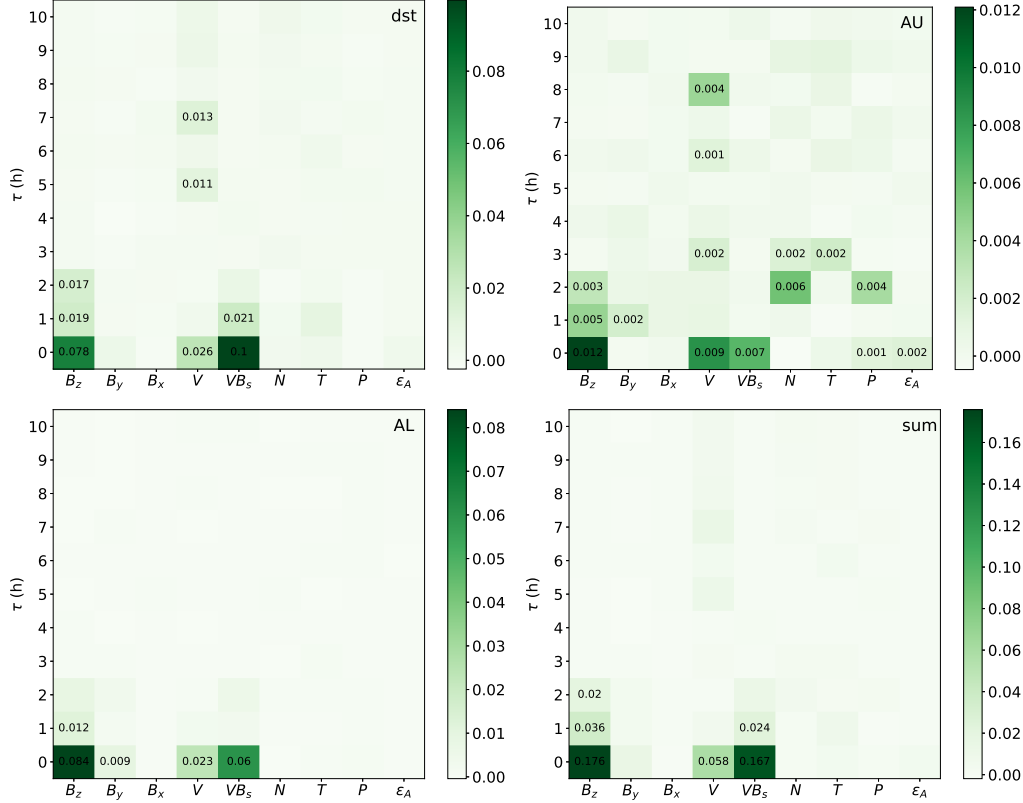


**Figure 5.** Summary of the response of the trained NNs to the randomization for each solar wind driver at each time delay  $\tau$  considered in the entry. We show the error on (a) Dst, (b) AL, (c) AU, and (d) Sum of the previous 3. We note that only a few variables are relevant.

249 an error range that shows how stable is the perturbation. If the bar is compatible with  
 250 0, we can conclude that the driver is globally not contributing to the prediction. A global  
 251 overview shows that the *Dst* index is the most sensitive to the solar wind drivers since  
 252 the error is clearly higher than AU or AL. AU is not convincing in its sensitivity to the  
 253 solar wind drivers, only  $B_z$  has a result not compatible with 0. From the point of view  
 254 of the solar wind variables, we see again that  $B_z$  and  $VB_s$  are picked up by strategy as  
 255 the most relevant solar wind variables to forecast the geomagnetic indices. The  $B_x$  and  
 256  $\epsilon_A$  variables do not bring significant information to the prediction while the error pro-  
 257 duced by  $B_y$ ,  $V$ ,  $N$ ,  $T$ , and  $P$  is quite reduced compared with the first two variables  $B_z$   
 258 and  $VB_s$ .

259 From now on, instead of adding an error to the signal we randomize the order of  
 260 the solar wind driver time series for a particular storm (a surrogate). Using this random-  
 261 ization input method, we can look deeper inside the solar wind drivers. We are not only  
 262 interested in identifying the solar wind variable that could contribute to predict the ge-  
 263 omagnetic indices, but also at which time  $t-\tau$  they should be taken to make a robust  
 264 prediction. In order to find the most relevant components  $I_{i,t-\tau}$  that affect the GI, we  
 265 test the selected NN for each SWV at a particular time delay and repeat the surrogate  
 266 randomizing procedure outlined above. Again, we expect that the most relevant com-  
 267 ponents are the ones that should degrade the prediction the most. This procedure will  
 268 produce one global associated error for each solar wind driver, at each time delay, of each  
 269 geomagnetic index and each storm. Hence, it will give us clues about which solar wind  
 270 drivers and delays should be used to construct a robust NN prediction model.

271 In Fig. 5a-c, we show the variation of the MAE produced by each component of  
 272 each solar wind driver up to 10 hrs before the last available measurement for each ge-  
 273 omagnetic index. We note that only a few solar wind variables, at particular time de-  
 274 lays, are robust variables. Figure 5d displays the sum of the MAE for the 3 geomagnetic  
 275 indices, providing a global descriptor of the robust solar wind drivers for this coupled  
 276 system. We consider that a component contributes to the prediction (i.e., is robust) when  
 277 it reaches 10% of the maximum value obtained in the matrix. For *Dst*,  $B_z$  is contribut-  
 278 ing up to 3 hours before the last measurement while  $VB_s$  only 2 hours. Some delayed  
 279 components of the speed signal also seem to bring a significant contribution to the pre-  
 280 diction. For AU, it looks that many components are turned on given the very low max-  
 281 imum, however, we can highlight the most important components being the immediate  
 282 measurements of  $B_z$ ,  $V$ , and  $VB_s$ . Finally AL has five components turned on, where again  
 283 the last value of  $B_z$  and  $VB_s$  seem to be the best contributors. The global sum of the  
 284 errors, shown in Fig. 5d, highlight 6 values which will be considered for our final robust  
 285 model, namely, the 3 previous values of  $B_z$ , the last value of  $V$ , and the two last values  
 286 of  $VB_s$ .

287 Once we have determined which are the most relevant solar wind drivers, at partic-  
 288 ular time delays, that drive the coupled geomagnetic indices, we train a robust NN  
 289 replacing  $\mathbf{I}_t$  by a vector containing those 6 components. Hence, we now retrain our NN  
 290 with the global entry containing the same geomagnetic indices but with the 6 outstand-  
 291 ing solar wind inputs of Fig. 5d. In parallel we build a linear model using the same en-  
 292 tries for comparison.

293 As a matter of testing, we also want to use iterated predictions for the NN and lin-  
 294 ear model, meaning that they have to use the geomagnetic values they predicted  $\bar{\mathbf{G}}_t$  in  
 295 the previous time step to produce the next predicted value, namely,

$$\bar{\mathbf{G}}_{t+1} = NN(\bar{\mathbf{G}}_{t+1}, \tilde{\mathbf{I}}_t),$$

296 where  $\tilde{\mathbf{I}}_t$  corresponds to the subset of 6 robust variables that are used as drivers of the  
 297 neural net. Such approach may be useful for real time forecasts when only solar wind  
 298 variables are available. One would naturally expect that the iterated predictions are less  
 299 accurate than the one step predictions, that uses previously measured  $\mathbf{G}_t$  values to drive  
 300 the neural net. However it becomes relevant to compare these results with an equiva-  
 301 lent model that does not consider the robustness of the variables. Therefore, as a way  
 302 to compare, we construct NN and linear models using the 11 last measurements of the  
 303 best driver  $B_z$  (left column of Fig. 5d). In Fig. 6a we plot the results over the valida-  
 304 tion set for the globally robust NN, while in Fig. 6b we show the results of the NN and  
 305 linear models that use only the  $B_z$  driver at all time delays (11 inputs to the neural net).  
 306 Each bin represents the normalized-by-persistence error for each geomagnetic index with  
 307 a deviation bar for the 20 storms of the validation set.

308 In the case of one step forecasting of the robust model, although existent, the im-  
 309 provement do not look significantly different for both linear and NN models, but when  
 310 we do iterated predictions the results becomes much more interesting. The prediction  
 311 of *Dst* by the globally robust NN model are 38% (14.3% for AL, and 17.0% for AU) bet-  
 312 ter than the linear model.

313 When comparing both robust and  $B_z$ -based nonlinear NN models, we find that for  
 314 *Dst* and *AU* the iterated globally robust forecast show a global improvement of 12.7%  
 315 and 8.7%, respectively, as compared with the  $B_z$ -based model. In the case of AL we ob-  
 316 tain no improvement. Note that we have used 6 solar wind entries for the robust model,  
 317 compared with the 11 solar wind entries of the  $B_z$ -based model. If we reduce the  $B_z$ -  
 318 based model to only just the first 6 time delays, the difference is more notorious with  
 319 respect to the robust model.

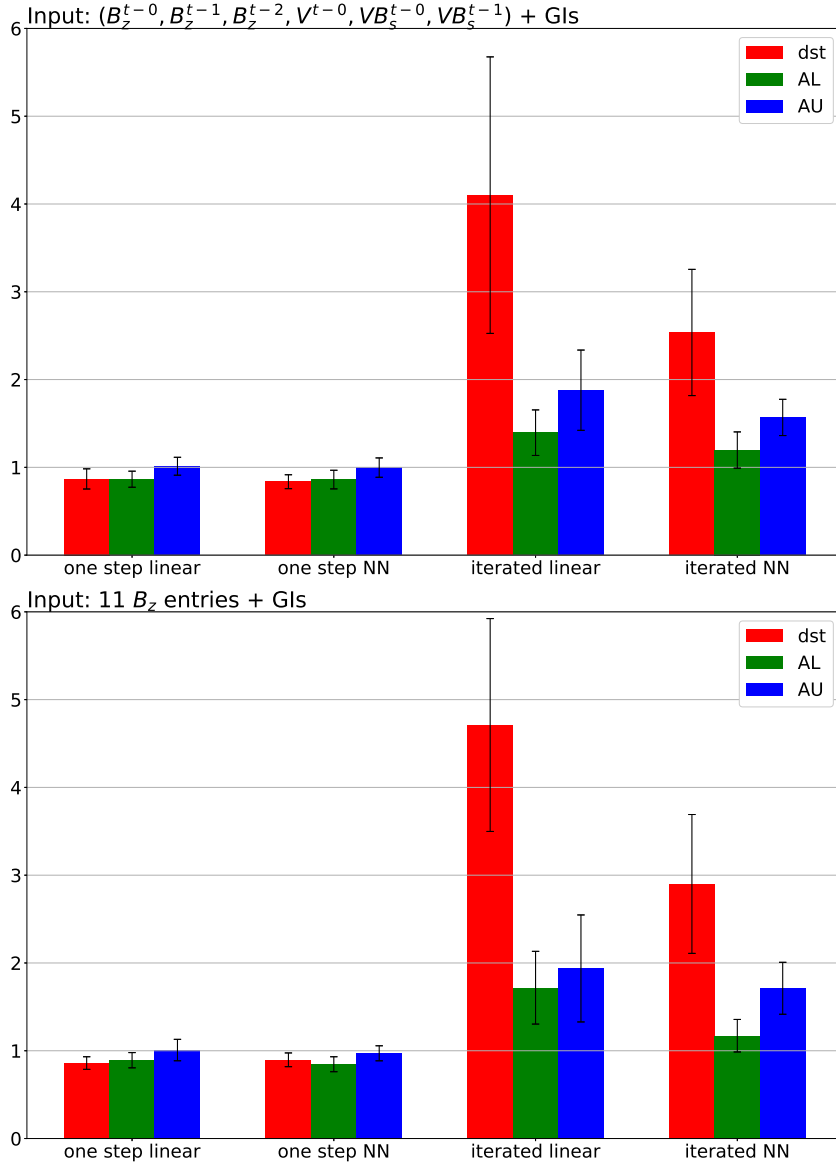


**Figure 6.** Normalized MAE for the (a) globally robust model, and (b) the model using the 11 last hours of  $B_z$ . We compare the NN versus a linear model using the same entries for one step and iterated predictions. The results are normalized with the error of the persistence. hence, the iterated forecasts using the nonlinear global robust model is an improvement from the equivalent model that uses only  $B_z$  variables, despite the fact that the later have a larger number of inputs (11 vs 6).

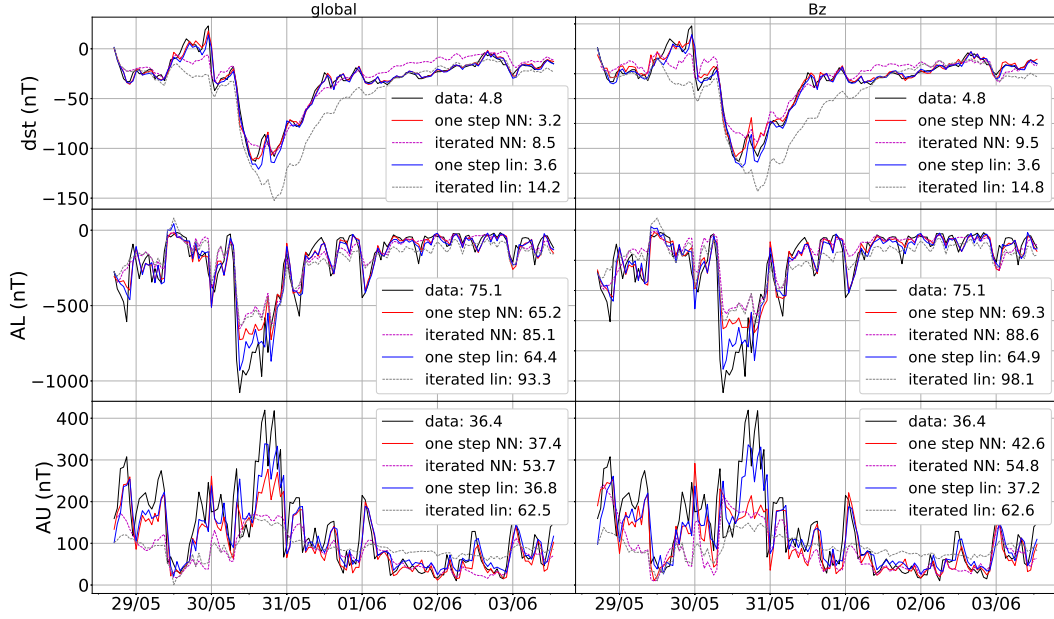


**Figure 7.** Forecasts of the geomagnetic indices during the storm of May 2005 for the (Left) Globally robust models and (Right) the  $B_z$  based models. The solid black line shows the data with a legend of MAE. Solid red (blue) corresponds to the one step prediction of NN (linear models).

320  
321  
322  
323  
324  
325  
326  
327  
328  
329  
330  
331

Figure 7 shows the one step and iterated globally robust model forecasting during the storm of May 2013 that reached a  $Dst$  minimum of  $-113\text{nT}$ . In the left panel we show the predictions for the globally robust NN and linear models and in the right panel we have results corresponding to the  $B_z$ -based models. The given numbers in the legend correspond to the bare MAE without normalization, and the errors of the different models (and one step vs. iterated) normalized to the persistence. The one step predictions show improvements from the  $B_z$  based model, for example  $Dst$  one step forecasting is improved by 23.8% when comparing the NN models. When looking at the iterated prediction, the globally robust model improves the  $Dst$  iterated prediction by 10.5% in this particular case. On the other hand, we highlight the notorious improvement for this storm of the error in  $Dst$  for the globally robust model of 40.1% between linear and NN models.

#### 4 Conclusions

332  
333  
334  
335  
336  
337  
338  
339  
340  
341  
342  
343  
344

We have studied the correlation between geomagnetic indices ( $Dst$ , AU and AL) and interplanetary solar wind variables at the L1 point of the Sun-Earth system through 64 geomagnetic storms, for which we have simultaneous data, that occurred since 1995. The method we used is based on training Neural Networks and look at their capability to predict the evolution of the magnetosphere in storm periods. We stressed the entries of the trained Neural Networks in order to evaluate their robustness of the solar wind variables, at particular time delays, in the prediction of the geomagnetic indices. The magnetic  $z$ -component of the interplanetary magnetic field and the duskward oriented component of the electric field  $VB_z$  appeared to be the most robust drivers for the prediction since the addition of a noise to them shown a significant degradation in their capacity to drive the geomagnetic indices. By a similar method we determined which of the 9 solar wind variables, and particular time delays, we must consider in this analy-

345 sis to give the best predictions of the geomagnetic indices. We obtain that the relevance  
 346 of the geomagnetic variables gets reduced considerably for  $t \leq 3$  hours from the last  
 347 measurement.

348 The pressure, the  $\epsilon_A$  parameter, the temperature, the  $x$  and  $y$  components of the  
 349 magnetic field, and the particle density of the interplanetary medium do not seem to bring  
 350 significant contribution to the prediction at this level of approximation.

351 Finally we built a linear and nonlinear models based on the robust solar wind vari-  
 352 ables in their capability to forecast. We show that over a sample of 20 storms, the fore-  
 353 casting of  $Dst$  is improved by 12.7% from a Neural Network based only on the interplan-  
 354 etary  $z$ -component of the magnetic field that consider 11 time delays. Neural network  
 355 are 38% better to predict  $Dst$  than linear models which emphasizes the highly non-linear  
 356 behavior of the magnetosphere. Hence, the robust model, with only its 6 solar wind drivers,  
 357 provides an improvement in the forecast of this simplified SWMI system representation.  
 358 Of course, we could consider including robust magnetospheric indices at various time de-  
 359 lays, as variables for the NN, a work that we plan to conduct in a future publication.

360 Future forecasting models of MIs should strongly consider the highlighted variables  
 361 and time delays as input of their models. This is in particular true for  $Dst$  forecasting  
 362 which is widely used to describe the state of the magnetosphere. Of course, additional  
 363 information is provided about AL and AU, which are in general hard to obtain in real  
 364 time. A similar method can be used to highlight the driving variables of other geomag-  
 365 netic indices, like  $K_p$  or  $A_p$ , used in web services in order to improve the reliability of  
 366 the forecasts. Those results can be used to construct step-by-step a multivariate, robust  
 367 system science, description of the magnetosphere evolution.

368 Moreover, variables that show significant contribution at several time delays can  
 369 be interpreted as orders in differential equation that can drive the MIs. Therefore it could  
 370 improve existing minimal system-science mathematical descriptions of the magnetosphere  
 371 behavior at the one hour time-scale.

372 It is worth noticing that the MI coupled model can be further used to test hypoth-  
 373 esis of cross-predictability among the MIs, by using measured sequences of a subset of  
 374 them to forecast, in an iterated scheme, the others by using the measured MIs as input  
 375 in the robust model proposed. Such analysis may help further our understanding of the  
 376 so called “storm-substorm” coupling. This will be presented shortly.

377 Finally, these type of techniques can be used to find the relevant drivers in other  
 378 nonlinear systems, where including too many variables in the NNs may be dangerous if  
 379 we intend to produce robust forecasts. We plan to introduce other magnetospheric in-  
 380 dices in a larger version of the SWMI system representation.

## 381 Acknowledgments

382 We acknowledge fruitful discussion with Joe Borovsky. We kindly thank the World Data  
 383 Center for Geomagnetism, to provide openly data of the  $Dst$  geomagnetic index used  
 384 in this study. We also acknowledge N. Papitashvili and J.King at the National Space Sci-  
 385 ence Data Center of the Goddard Space Flight Center for the use permission of 1 min  
 386 OMNI data and the NASA CDAWeb team for making these data available. We thank  
 387 the support of Fondecyt Grant No. 1190703, US ASFOR Award No. FA9550-18-1-0438,  
 388 and US ASFOR Award No. FA9550-19-1-0384.

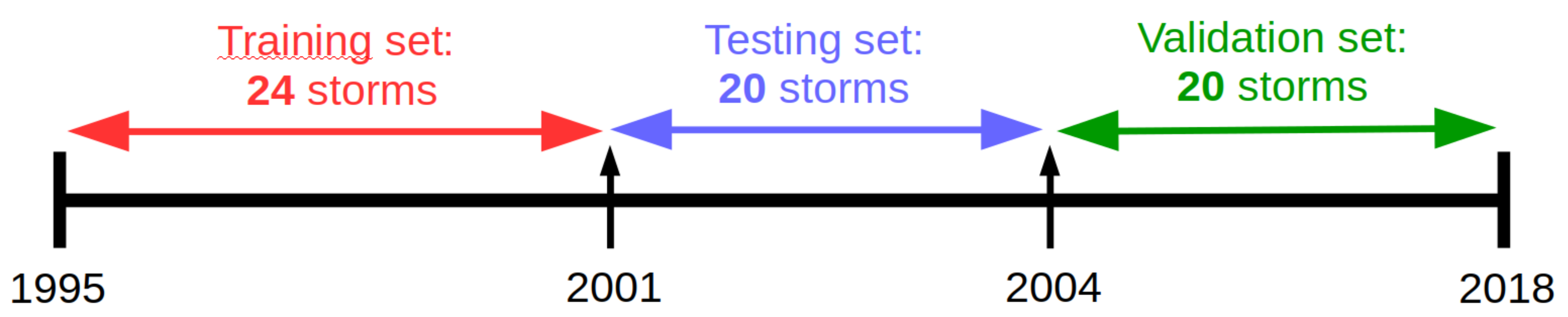
## 389 References

390 Abiodun, O. I., Jantan, A., Omolara, A. E., Dada, K. V., Mohamed, N. A., &  
 391 Arshad, H. (2018). State-of-the-art in artificial neural network applica-

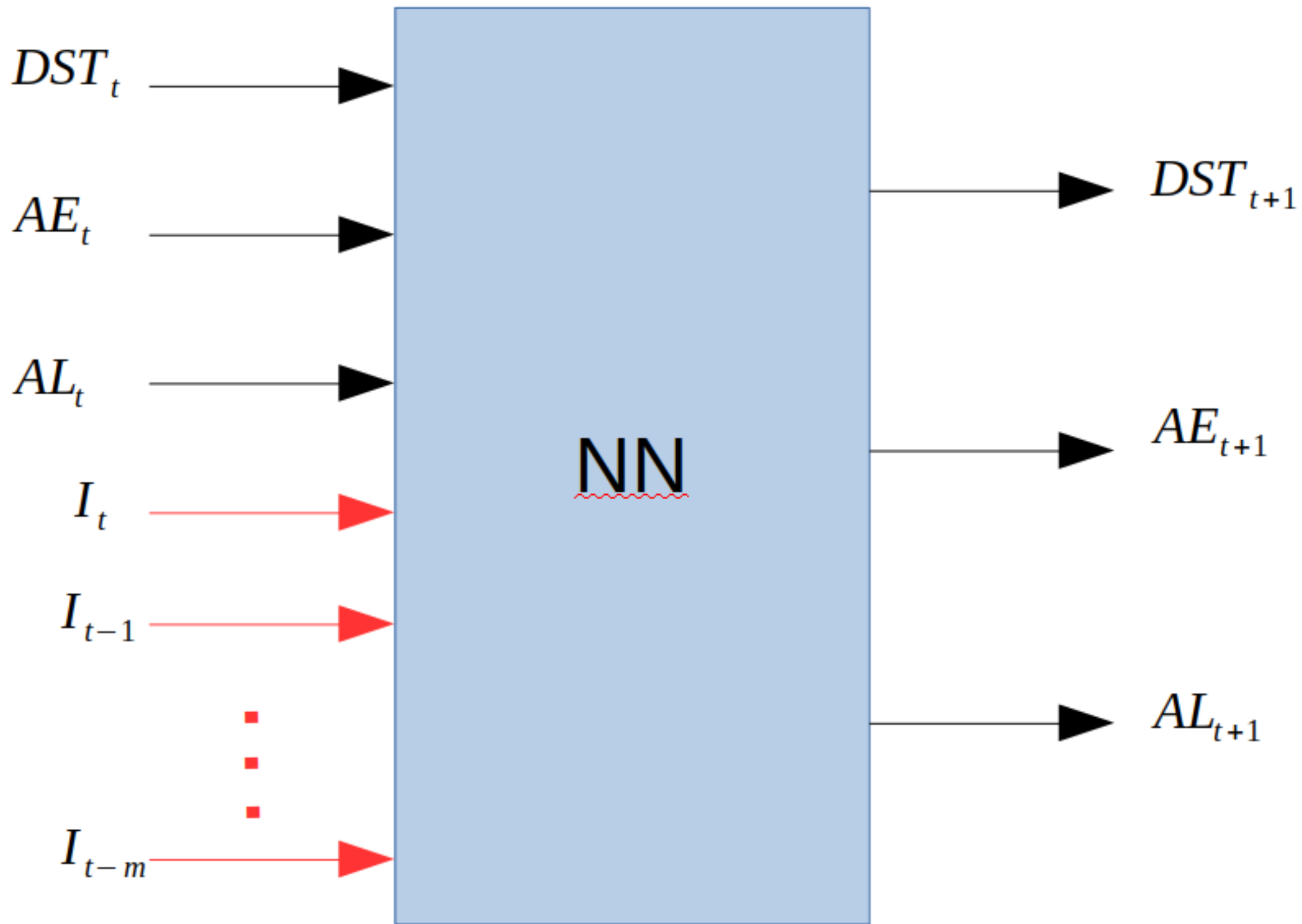
- 392 tions: A survey. *Heliyon*, 4(11), e00938. doi: [https://doi.org/10.1016/](https://doi.org/10.1016/j.heliyon.2018.e00938)  
393 [j.heliyon.2018.e00938](https://doi.org/10.1016/j.heliyon.2018.e00938)
- 394 Adhikari, B., Sapkota, N., Dahal, S., Bhattarai, B., Khanal, K., & Chapagain, N.  
395 (2020, 06). Spectral characteristic of geomagnetically induced current during  
396 geomagnetic storms by wavelet techniques.
- 397 Bala, R., & Reiff, P. (2018). Chapter 2 - data availability and forecast products  
398 for space weather. In E. Camporeale, S. Wing, & J. R. Johnson (Eds.),  
399 *Machine learning techniques for space weather* (p. 27 - 41). Elsevier. Re-  
400 trieved from [http://www.sciencedirect.com/science/article/pii/](http://www.sciencedirect.com/science/article/pii/B978012811788000020)  
401 [B978012811788000020](http://www.sciencedirect.com/science/article/pii/B978012811788000020) doi: [https://doi.org/10.1016/B978-0-12-811788-0](https://doi.org/10.1016/B978-0-12-811788-0.00002-0)  
402 [.00002-0](https://doi.org/10.1016/B978-0-12-811788-0.00002-0)
- 403 Bargatze, L. F., Baker, D. N., L., M. R., & Hones, E. W. (1985). Magnetospheric re-  
404 sponse to the imf: substorms. *Journal of Geophysical Research: Space Physics*,  
405 90, 6387.
- 406 Borovsky, J. E. (2020). A survey of geomagnetic and plasma time lags in  
407 the solar-wind-driven magnetosphere of earth. *Journal of Atmospheric*  
408 *and Solar-Terrestrial Physics*, 208, 105376. Retrieved from [http://](http://www.sciencedirect.com/science/article/pii/S1364682620301875)  
409 [www.sciencedirect.com/science/article/pii/S1364682620301875](http://www.sciencedirect.com/science/article/pii/S1364682620301875) doi:  
410 <https://doi.org/10.1016/j.jastp.2020.105376>
- 411 Borovsky, J. E., & Denton, M. H. (2018). Exploration of a composite index to de-  
412 scribe magnetospheric activity: Reduction of the magnetospheric state vector  
413 to a single scalar. *Journal of Geophysical Research: Space Physics*, 123(9),  
414 7384-7412. doi: 10.1029/2018JA025430
- 415 Borovsky, J. E., & Shprits, Y. Y. (2017). Is the dst index sufficient to define all  
416 geospace storms? *Journal of Geophysical Research: Space Physics*, 122(11),  
417 11,543-11,547. doi: 10.1002/2017JA024679
- 418 Borovsky, J. E., & Valdivia, J. A. (2018). The earth's magnetosphere: A systems  
419 science overview and assessment. *Surveys of Geophysics*, 39(11), 817. doi: 10  
420 [.1007/s10712-018-9487-x](https://doi.org/10.1007/s10712-018-9487-x)
- 421 Bortnik, J., Chu, X., Ma, Q., Li, W., Zhang, X., Thorne, R. M., ... Baker, D. N.  
422 (2018). Chapter 11 - artificial neural networks for determining magneto-  
423 spheric conditions. In E. Camporeale, S. Wing, & J. R. Johnson (Eds.),  
424 *Machine learning techniques for space weather* (p. 279 - 300). Elsevier.  
425 Retrieved from [http://www.sciencedirect.com/science/article/pii/](http://www.sciencedirect.com/science/article/pii/B978012811788000111)  
426 [B978012811788000111](http://www.sciencedirect.com/science/article/pii/B978012811788000111) doi: [https://doi.org/10.1016/B978-0-12-811788-0](https://doi.org/10.1016/B978-0-12-811788-0.00011-1)  
427 [.00011-1](https://doi.org/10.1016/B978-0-12-811788-0.00011-1)
- 428 Burton, R. K., McPherron, R. L., & Russell, C. T. (1975). An empirical relationship  
429 between interplanetary conditions and dst. *Journal of Geophysical Research:*  
430 *Space Physics*, 80, 4204.
- 431 Camporeale, E. (2019). The challenge of machine learning in space weather:  
432 Nowcasting and forecasting. *Space Weather*, 17(8), 1166-1207. Retrieved  
433 from [https://agupubs.onlinelibrary.wiley.com/doi/abs/10.1029/](https://agupubs.onlinelibrary.wiley.com/doi/abs/10.1029/2018SW002061)  
434 [2018SW002061](https://agupubs.onlinelibrary.wiley.com/doi/abs/10.1029/2018SW002061) doi: 10.1029/2018SW002061
- 435 Consolini, G., Alberti, T., & De Michelis, P. (2018). On the forecast horizon of mag-  
436 netospheric dynamics: A scale-to-scale approach. *Journal of Geophysical Re-*  
437 *search: Space Physics*, 123(11), 9065-9077. doi: 10.1029/2018JA025952
- 438 Council, N. R. (2008). *Severe space weather events: Understanding societal and eco-*  
439 *nomic impacts: A workshop report*. Washington, DC: The National Academies  
440 Press. Retrieved from [https://www.nap.edu/catalog/12507/severe-space](https://www.nap.edu/catalog/12507/severe-space-weather-events-understanding-societal-and-economic-impacts-a)  
441 [-weather-events-understanding-societal-and-economic-impacts-a](https://www.nap.edu/catalog/12507/severe-space-weather-events-understanding-societal-and-economic-impacts-a) doi:  
442 [10.17226/12507](https://doi.org/10.17226/12507)
- 443 Davis, T. N., & Sugiura, M. (1966). Auroral electrojet activity index ae and its  
444 universal time variations. *Journal of Geophysical Research (1896-1977)*, 71(3),  
445 785-801. doi: 10.1029/JZ071i003p00785
- 446 Donner, R. V., Balasis, G., Stolbova, V., Georgiou, M., Wiedermann, M., & Kurths,

- 447 J. (2019). Recurrence-based quantification of dynamical complexity in the  
 448 earth's magnetosphere at geospace storm timescales. *Journal of Geophysical*  
 449 *Research: Space Physics*, *124*(1), 90-108. doi: 10.1029/2018JA025318
- 450 Gosling, J. T. (2000). The solar flare myth. *Journal of Geophysical Research: Space*  
 451 *Physics*, *98*, 18937.
- 452 Gruet, M. A., Chandorkar, M., Sicard, A., & Camporeale, E. (2018). Multiplehour-  
 453 ahead forecast of the dst index using a combination of long short-term memory  
 454 neural network and gaussian process. *Space Weather*, *16*, 1882-1896. doi:  
 455 10.1029/2018SW001898
- 456 Hapgood, M. (2018). Chapter 1 - societal and economic importance of space  
 457 weather. In E. Camporeale, S. Wing, & J. R. Johnson (Eds.), *Machine learn-*  
 458 *ing techniques for space weather* (p. 3 - 26). Elsevier. Retrieved from [http://](http://www.sciencedirect.com/science/article/pii/B9780128117880000019)  
 459 [www.sciencedirect.com/science/article/pii/B9780128117880000019](http://www.sciencedirect.com/science/article/pii/B9780128117880000019)  
 460 doi: <https://doi.org/10.1016/B978-0-12-811788-0.00001-9>
- 461 Jawad, M., Rafique, A., Khosa, I., Ghous, I., Akhtar, J., & Ali, S. M. (2019, Feb).  
 462 Improving disturbance storm time index prediction using linear and nonlinear  
 463 parametric models: A comprehensive analysis. *IEEE Transactions on Plasma*  
 464 *Science*, *47*(2), 1429-1444. doi: 10.1109/TPS.2018.2887202
- 465 King, J. H., & Papitashvili, N. E. (2005). Solar wind spatial scales in and compar-  
 466 isons of hourly wind and ace plasma and magnetic field data. *Journal of Geo-*  
 467 *physical Research: Space Physics*, *110*(A2). Retrieved from [https://agupubs](https://agupubs.onlinelibrary.wiley.com/doi/abs/10.1029/2004JA010649)  
 468 [.onlinelibrary.wiley.com/doi/abs/10.1029/2004JA010649](https://agupubs.onlinelibrary.wiley.com/doi/abs/10.1029/2004JA010649) doi: 10.1029/  
 469 2004JA010649
- 470 Lazzus, J. A., Vega, P., Rojas, P., & Salfate, I. (2017). Forecasting the dst index us-  
 471 ing a swarm-optimized neural network. *Space Weather*, *15*(8), 1068-1089. doi:  
 472 10.1002/2017SW001608
- 473 Masahito, N., Sugiura Masahisa, Kamei Toyohisa, Iyemori Toshihiko, & Yukinobu,  
 474 K. (2015). *Dst index*. WDC for Geomagnetism, Kyoto. Retrieved from  
 475 [http://isds-datadoi.nict.go.jp/wds/10.17593\\_14515-74000.html](http://isds-datadoi.nict.go.jp/wds/10.17593_14515-74000.html) doi:  
 476 10.17593/14515-74000
- 477 Sugiura, M. (1964, 1). Hourly values of equatorial dst for the igy. *Ann. Int. Geo-*  
 478 *phys. Yr.*, *35*.
- 479 Valdivia, J., Rogan, J., Munoz, V., Toledo, B. A., & Stepanova, M. (2013). The  
 480 magnetosphere as a complex system. *Advances of Space Research*, *51*, 1934.
- 481 Valdivia, J. A., Rogan, J., Munoz, V., Gomberoff, L., Klimas, A. J., Vassiliadis, D.,  
 482 ... Wastavino, B. T. L. (2005). The magnetosphere as a complex system.  
 483 *Advances of Space Research*, *35*, 961-971.
- 484 Valdivia, J. A., Sharma, A. S., & Papadopoulos, K. (1996). Prediction of magnetic  
 485 storms by nonlinear models. *Geophysical Research Letters*, *23*(21), 2899-2902.  
 486 doi: 10.1029/96GL02828
- 487 Valdivia, J. A., Vassiliadis, D., & Klimas, A. J. (1999). Modeling the spatial struc-  
 488 ture of the high latitude magnetic perturbation in the related current system.  
 489 *Physics of Plasmas*, *6*, 4185-4194.
- 490 Vassiliadis, D., Klimas, A. J., Baker, D. N., & Roberts, D. A. (1995). A description  
 491 of the solar wind-magnetosphere coupling based on nonlinear filters. *Journal of*  
 492 *Geophysical Research: Space Physics*, *100*, 3495-3512.
- 493 Vassiliadis, D., Klimas, A. J., Valdivia, J. A., & Baker, D. N. (1999). The dst ge-  
 494 omagnetic response as a function of storm phase and amplitude and the solar  
 495 wind electric field. *Journal of Geophysical Research: Space Physics*, *104*,  
 496 24957.
- 497 Vassiliadis, D., Klimas, A. J., Valdivia, J. A., & Baker, D. N. (2000). The nonlinear  
 498 dynamics of space weather. *Advances of Space Research*, *26*, 197.

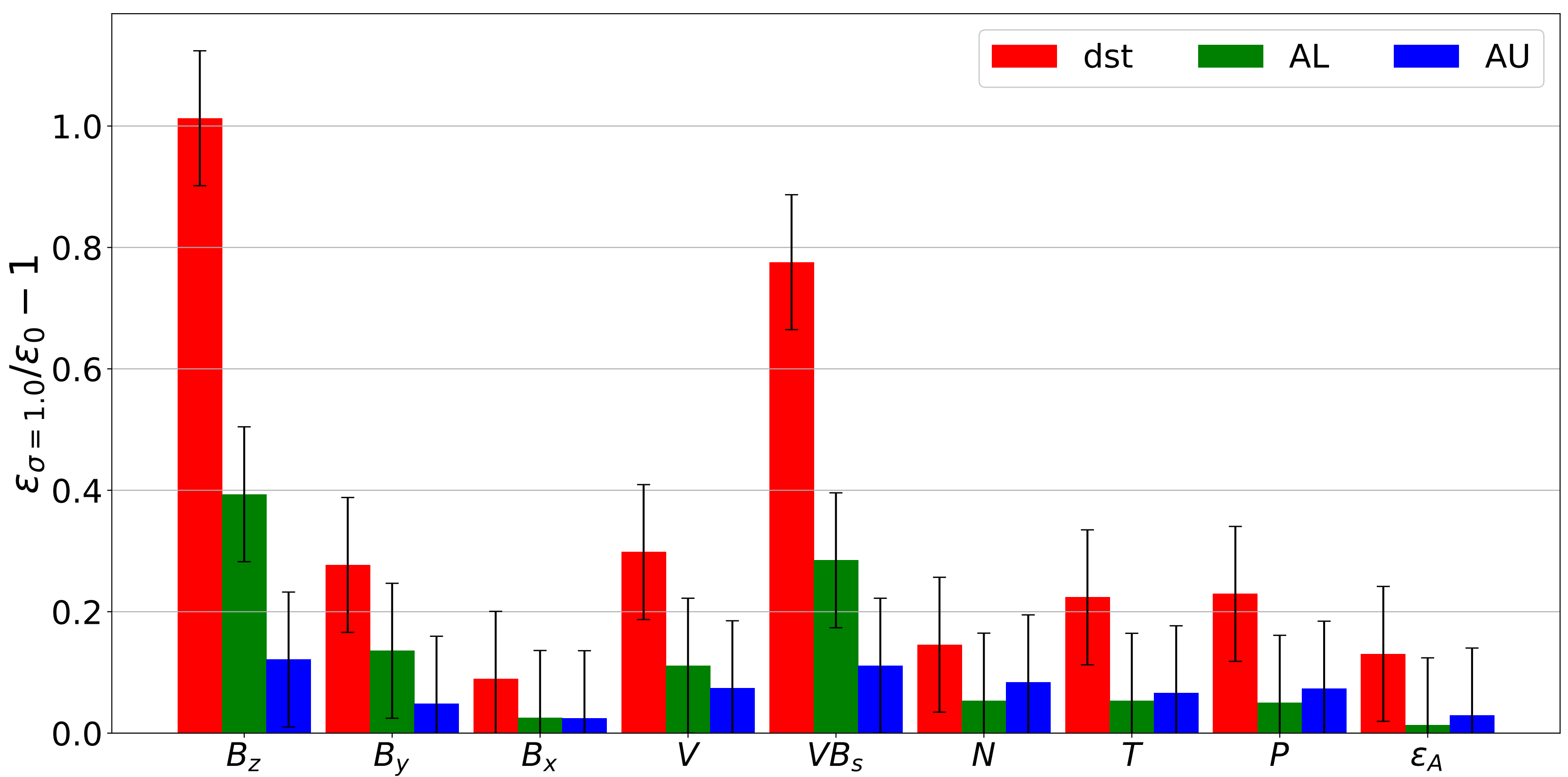
**data\_set\_repartition.**



**NN\_representation.**



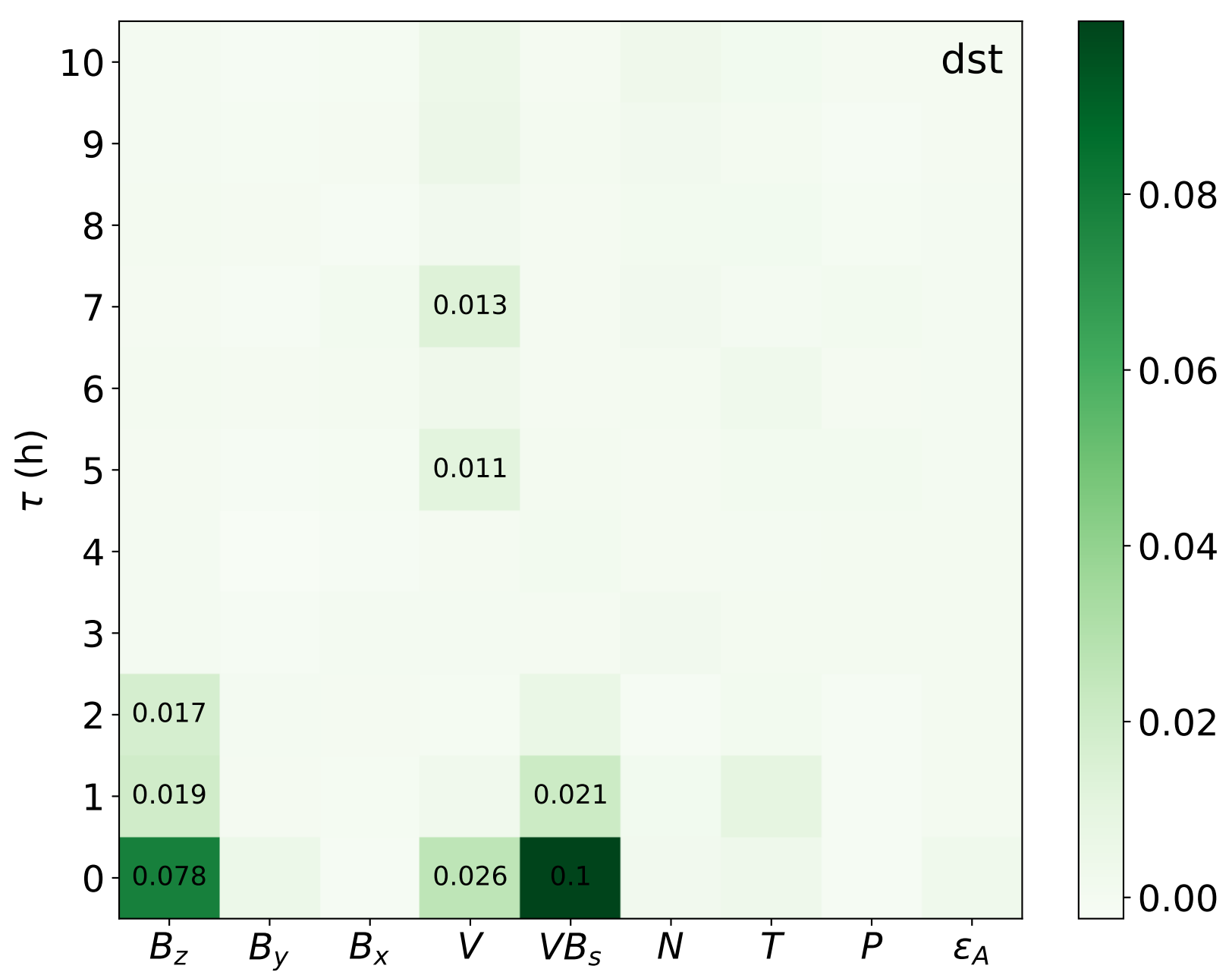
sigma.



AU\_tau.



dst\_tau.



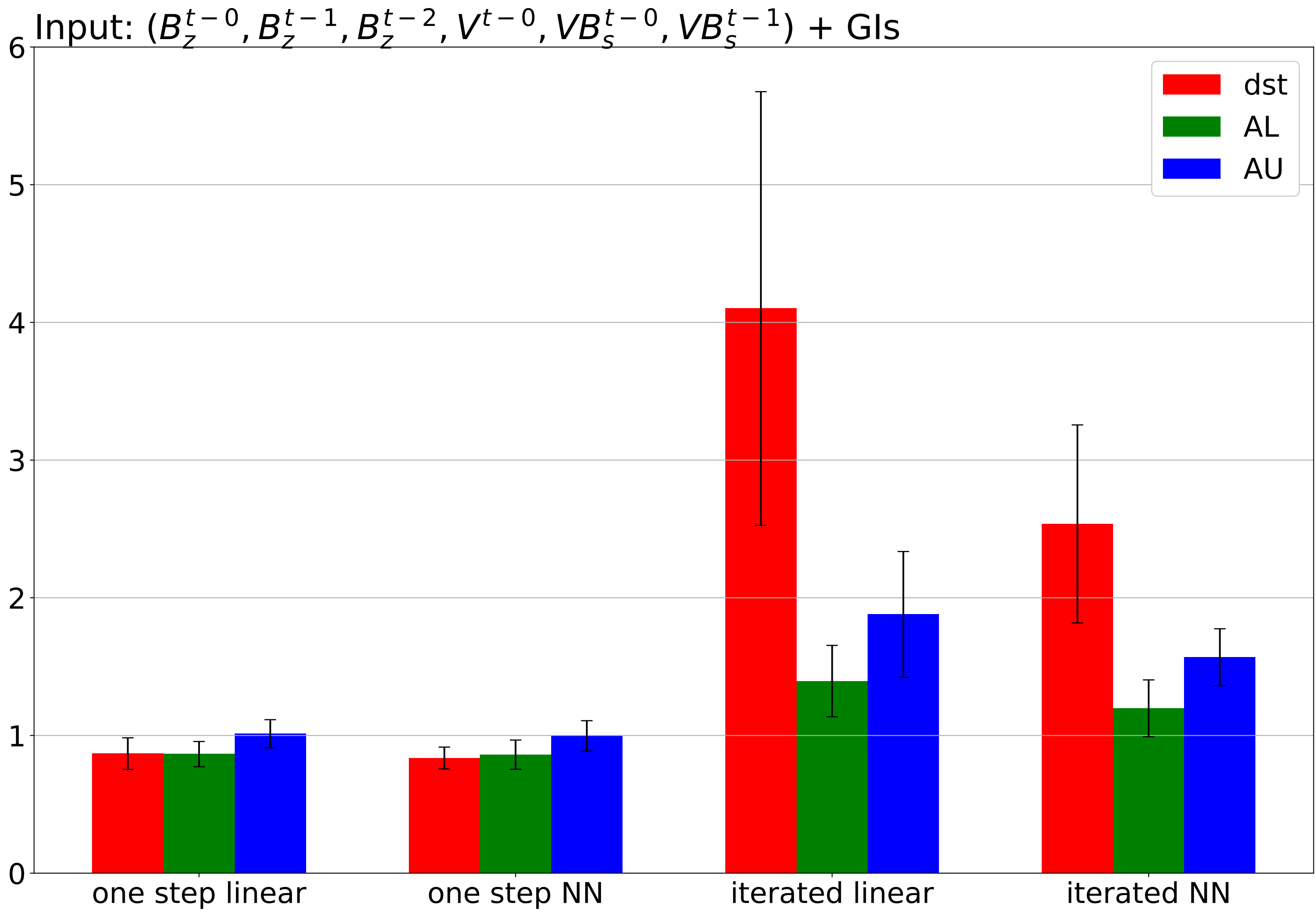
AL\_tau.



sum\_histog.



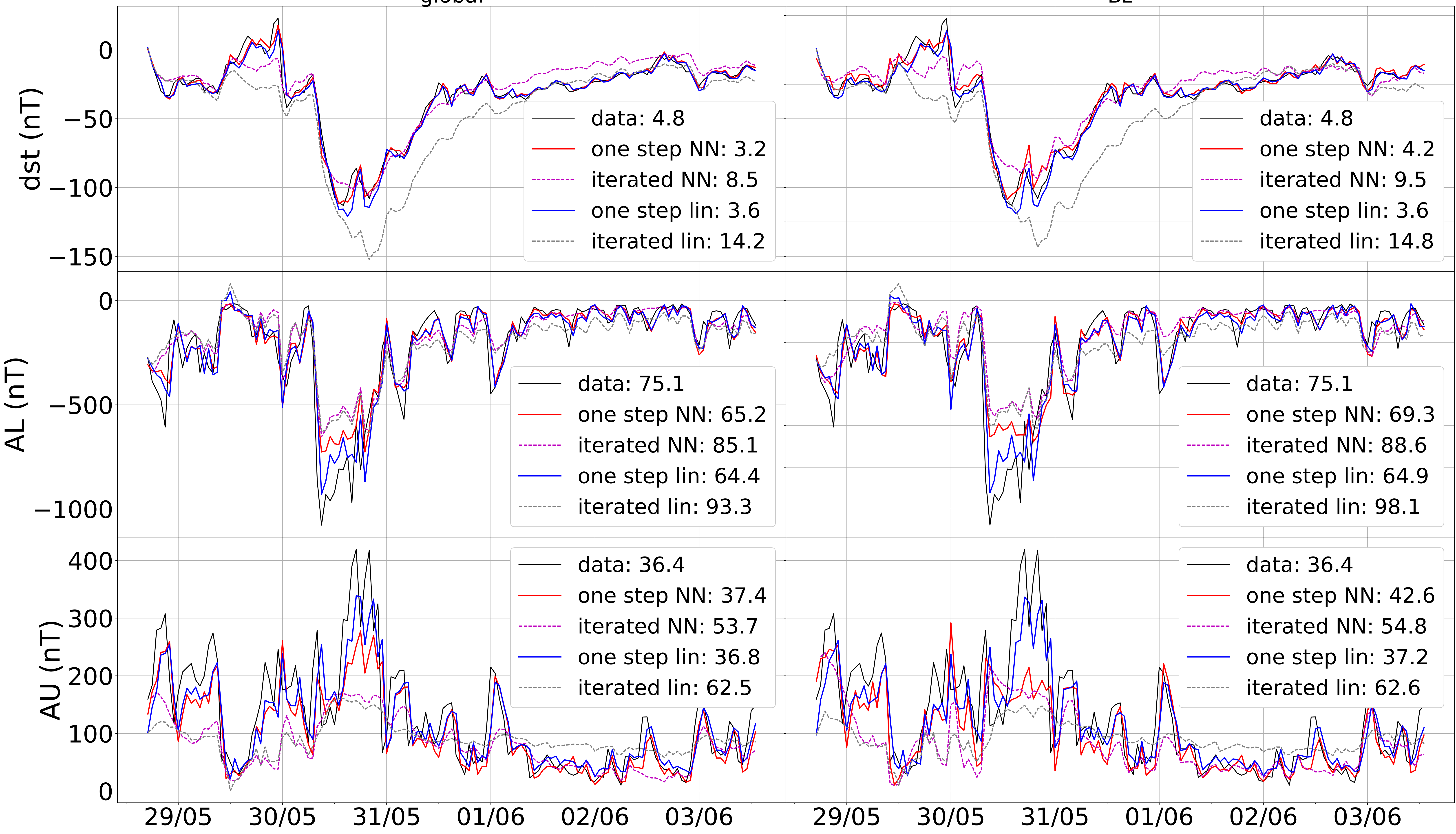
global\_validation\_histog\_ND.



20050530.

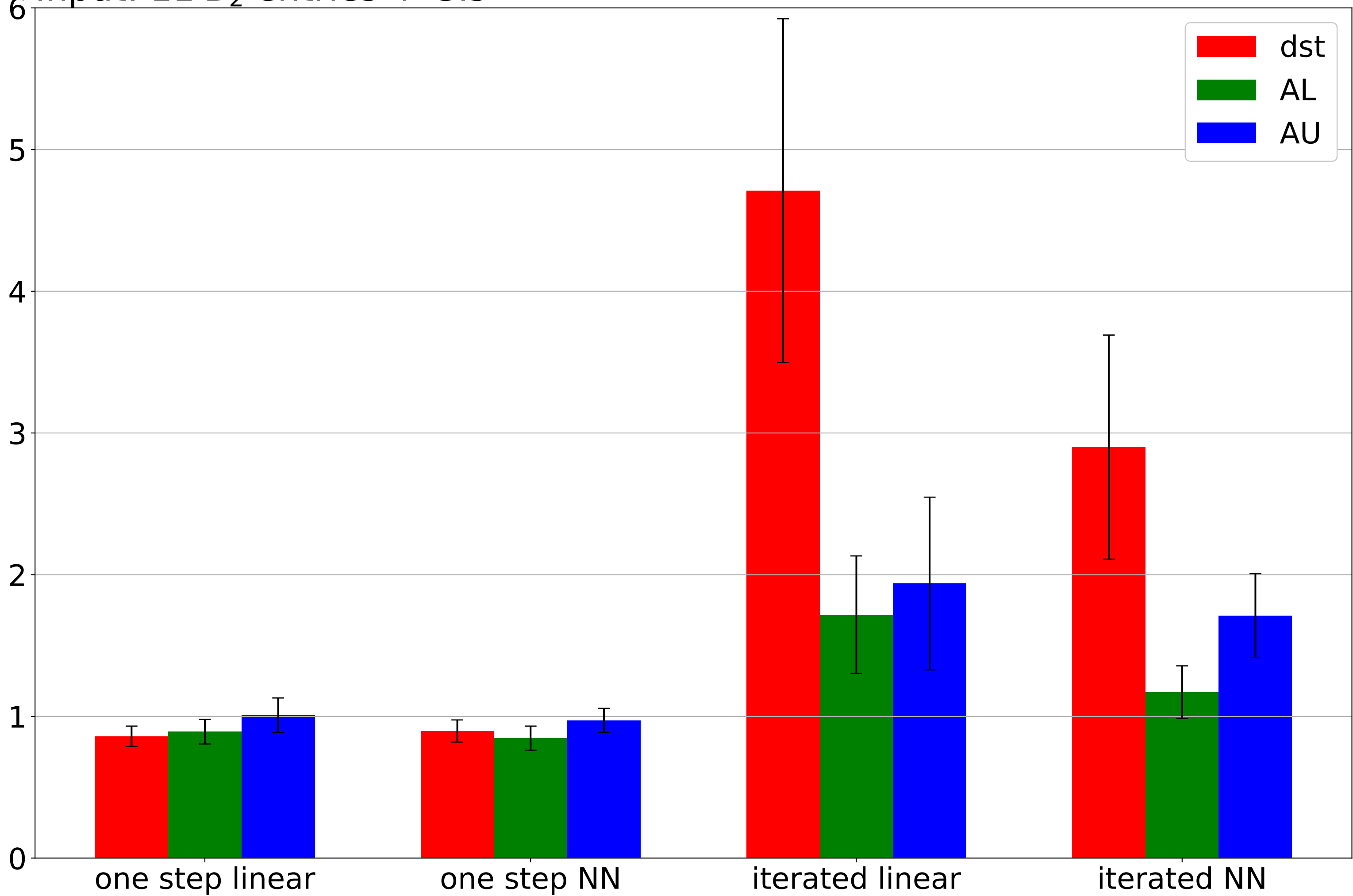
global

Bz



Bz\_validation\_histog.

Input: 11  $B_z$  entries + GIs



onestep\_20010320.

